Journal of Science and Transport Technology
Journal homepage: https://jstt.vn/index.php/en

Postbuckling analysis of externally pressured parabola, sinusoidal and cylindrical FG-GRCL panels using HSDT

Nguyen Thi Phuong[1,2], Cao Van Doan[3], Vu Hoai Nam[3,*]

[1]Computational Laboratory for Advanced Materials and Structures, Advanced Institute of Materials Science, Ton Duc Thang University, Ho Chi Minh City 70000, Vietnam, nguyenthiphuong@tdtu.edu.vn

[2]Faculty of Civil Engineering, Ton Duc Thang University, Ho Chi Minh City 70000, Vietnam

[3]Faculty of Civil Engineering, University of Transport Technology, Hanoi 10000, Vietnam

Article info
Type of article:
Original research paper

DOI:
https://doi.org/10.58845/jstt.utt.2023.en.3.2.34-43

***Corresponding author:**
E-mail address:
hoainam.vu@utt.edu.vn

Received: 25/05/2023
Revised: 26/06/2023
Accepted: 28/06/2023

Abstract: In the present paper, by using the higher-order shear deformation theory and the strain-displacement relationships of large deflection, the postbuckling analysis of the functionally graded graphene-reinforced composite laminated (FG-GRCL) parabola, sinusoidal, and cylindrical externally pressured panels is presented in detail. The complex curvature functions of the parabola and sinusoidal panels are considered. The stress function is approximately determined and the Galerkin process is utilized to achieve the stability equations of nonlinear problem. The expression of pressure-deflection postbuckling behavior can be explicitly obtained. The influences of curvature types, material properties, and geometric characteristics on the postbuckling behavior of panels are also considered and investigated.

Keywords: Postbuckling analysis; Cylindrical panel; Parabola panel; Sinusoidal panel; Higher-order shear deformation theory.

1. Introduction

Representative structures such as plates and cylindrical panels are utilized widely in the mechanical, space, and civil technologies. The functionally graded graphene-reinforced composite laminated (FG-GRCL) structures have attracted many scientists interested in research in recent years. By using the perturbed method with two steps and higher-order shear deformation theory (HSDT), the large-deflection bending, thermal and mechanical buckling of nonlinear problem, forced vibration of FG-GRCL cylindrical panels and plates were analyzed [1-4]. Vibration and postbuckling of FG-GRCL plates under thermal loads were calculated utilizing NURBS formulations [5-7] using the first-order shear deformation theory [5], and HSDT [6,7]. Nam et al. [8,9] and Phuong et al. [10,11] used the HSDT, Galerkin method, and the improved homogeneous techniques of stiffened structures to investigate the nonlinear buckling and postbuckling behavior of FG-GRCL plates and cylindrical panels with FG-GRCL stiffeners. In the authors' opinion, no research exists about external pressured parabola and sinusoidal FG-GRC panels. Thus, this paper studies postbuckling analysis of externally

pressured parabola, sinusoidal, and cylindrical FG-GRCL panels. The complex functions of curvatures of panels are the mathematical difficulty to determine the stress function form, and the approximate technique to obtain the stress function is utilized. The nonlinear formulations of the structures are formulated by using the HSDT and applying Galerkin process. The notable influences of the panel kind, graphene distribution rule, and geometric dimension on the postbuckling bearing capacity of the structures are initiated and examined.

2. Research method

The calculation process of this problem can be resumed in three steps: Firstly, the equilibrium equations are established utilizing the HSDT. Secondly, the compatibility and stress function is introduced. Next, the boundary conditions of problems are presented, and the forms of deflection and rotations are proposed. The stress function is determined with the utilization of an approximate technique. Finally, the Galerkin method is utilized to solve the obtained equations of the problem.

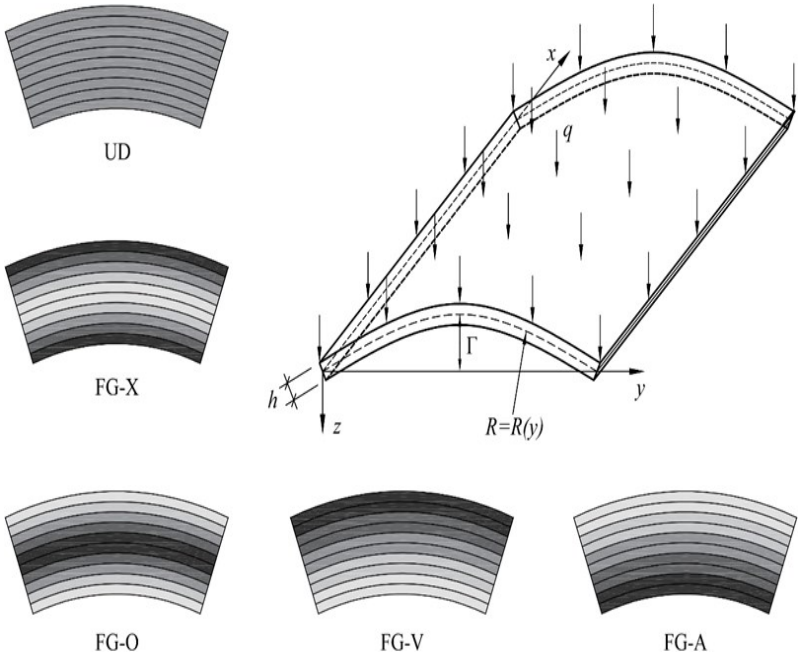

Fig. 1. Geometric dimensions and coordinate systems of parabola, sinusoidal, and cylindrical FG-GRCL panels

Configurations and material characteristics of parabola, sinusoidal, and cylindrical FG-GRCL panels are considered in this section. a, b, h, and Γ are the denotes of the length of edges, thickness, and maximum rise of curved mid-surface, respectively. The $Oxyz$ coordinate system is utilized, where the plane view of middle surface is on the Oxy plane and z is thickness direction as shown in Fig. 1.

The equations of the rise of mid-surface for the parabola and sinusoidal panels are presented as

$$r_{para} = y\frac{4\Gamma}{b} - y^2\frac{4\Gamma}{b^2}, r_{sin} = \left[\sin\left(\frac{\pi y}{b}\right)\right]\Gamma. \quad (1)$$

The radius functions R_1, and R_2 of the parabola and sinusoidal panels are obtained, respectively, as

$$R_1 = \frac{\left(16\Gamma^2(2y-b)^2 + b^4\right)^{3/2}}{8\Gamma b^4},$$
$$R_2 = \frac{\left(b^2 + \Gamma^2\pi^2\left(\cos\left(\frac{\pi y}{b}\right)\right)^2\right)^{3/2}}{\pi^2\Gamma b\sin\left(\frac{\pi y}{b}\right)}. \quad (2)$$

Two cases of directional placement of the graphene sheets in the polymeric matrix are defined as: the armchair edges are in the longitudinal axis (90-layer), and the zigzag edges are in the longitudinal axis (0-layer). Three arrangements $(0)_{10T}$, $(0/90/0/90/0)_S$ and $(0/90)_{5T}$, are created. Moreover, for the graphene volume fraction, three distributions UD, FG-X, and FG-O are assessed (Fig. 1).

Due to the nanoscale effectiveness, the effective parameters η_1, η_2 and η_3 are instituted [1-4] into Halpin-Tsai model to obtain the elastic and shear moduli of layers, as

$$E_1 = \frac{2V_G\gamma_1^G\frac{a_G}{h_G}+1}{1-V_G\gamma_1^G}E^m\eta_1,$$
$$E_2 = \frac{2V_G\gamma_2^G\frac{b_G}{h_G}+1}{1-V_G\gamma_2^G}E^m\eta_2,\quad G_{12} = \frac{G^m\eta_3}{1-V_G\gamma_{12}^G}, \tag{3}$$

with

$$\gamma_{11}^G = \frac{\frac{E_{11}^G}{E^m}-1}{\frac{E_{11}^G}{E^m}+2\frac{a_G}{h_G}},$$
$$\gamma_{22}^G = \frac{\frac{E_{22}^G}{E^m}-1}{\frac{E_{22}^G}{E^m}+2\frac{b_G}{h_G}},\qquad \gamma_{12}^G = \frac{\frac{G_{12}^G}{G^m}-1}{\frac{G_{12}^G}{G^m}}, \tag{4}$$

where the sub- of super-script m and G emblem matrix and graphene. b_G is the graphene width, a_G is the graphene length, and h_G is the graphene thickness. The shear and elastic moduli of graphene are symbolized by G_{12}^G, E_{11}^G, and E_{22}^G, respectively.

The Poisson ratio of GRCL panels is surmised as [1-4]

$$\nu_{12} = V_G\nu_{12}^G + V_m\nu^m. \tag{5}$$

The strain-displacement relations with the von Karman nonlinearities are presented as [2,3,9,11]

$$\begin{Bmatrix}\varepsilon_x\\ \varepsilon_y\\ \gamma_{xy}\end{Bmatrix} = \begin{Bmatrix}\varepsilon_x^0\\ \varepsilon_y^0\\ \gamma_{xy}^0\end{Bmatrix} + z\begin{Bmatrix}\varepsilon_x^1\\ \varepsilon_y^1\\ \gamma_{xy}^1\end{Bmatrix} + z^3\begin{Bmatrix}\varepsilon_x^3\\ \varepsilon_y^3\\ \gamma_{xy}^3\end{Bmatrix},$$
$$\begin{Bmatrix}\gamma_{xz}\\ \gamma_{yz}\end{Bmatrix} = \begin{Bmatrix}\gamma_{xz}^0\\ \gamma_{yz}^0\end{Bmatrix} + z^2\begin{Bmatrix}\gamma_{xz}^2\\ \gamma_{yz}^2\end{Bmatrix}, \tag{6}$$

where

$$\begin{Bmatrix}\varepsilon_x^0\\ \varepsilon_y^0\\ \gamma_{xy}^0\end{Bmatrix} = \begin{Bmatrix}u_{,x}+0.5w_{,x}^2+w_{,x}w_{0,x}\\ v_{,y}+0.5w_{,y}^2+w_{,y}w_{0,y}-w/R\\ v_{,x}+u_{,y}+w_{,x}w_{,y}+w_{,y}w_{0,x}+w_{,x}w_{0,y}\end{Bmatrix}, \tag{7}$$
$$\begin{Bmatrix}\gamma_{xz}^0\\ \gamma_{yz}^0\end{Bmatrix} = \begin{Bmatrix}w_{,x}+\phi_x\\ w_{,y}+\phi_y\end{Bmatrix}, \lambda = 4/3h^2$$

$$\begin{Bmatrix}\varepsilon_x^1\\ \varepsilon_y^1\\ \gamma_{xy}^1\end{Bmatrix} = \begin{Bmatrix}\phi_{x,x}\\ \phi_{y,y}\\ \phi_{y,x}+\phi_{x,y}\end{Bmatrix}, \begin{Bmatrix}\gamma_{xz}^2\\ \gamma_{yz}^2\end{Bmatrix} = -3\lambda\begin{Bmatrix}w_{,x}+\phi_x\\ w_{,y}+\phi_y\end{Bmatrix},$$
$$\begin{Bmatrix}\varepsilon_x^3\\ \varepsilon_y^3\\ \gamma_{xy}^3\end{Bmatrix} = -\lambda\begin{Bmatrix}w_{,xx}+\phi_{x,x}\\ w_{,yy}+\phi_{y,y}\\ \phi_{x,y}+2w_{,xy}+\phi_{y,x}\end{Bmatrix}, \tag{8}$$

and $w_0 = w_0(x,y)$ is the imperfection function of FG-GRCL panels.

The strain compatibility equation is received from Eq. (7), as

$$\varepsilon_{x,yy}^0+\varepsilon_{y,xx}^0-\gamma_{xy,xy}^0 = 2w_{,xy}w_{0,xy}-w_{,xx}w_{0,yy} - w_{,xx}w_{,yy}-w_{0,xx}w_{,yy}+w_{,xy}^2-\frac{w_{,xx}}{R}. \tag{9}$$

Hooke's law for the FG-GRCL panels considering the temperature effect is defined as [2,3,9,11]

$$\begin{bmatrix}\sigma_x\\ \sigma_y\\ \sigma_{xy}\\ \sigma_{xz}\\ \sigma_{yz}\end{bmatrix} = \begin{bmatrix}Q_{11}&Q_{12}&0&0&0\\ Q_{12}&Q_{22}&0&0&0\\ 0&0&Q_{66}&0&0\\ 0&0&0&Q_{44}&0\\ 0&0&0&0&Q_{55}\end{bmatrix}\begin{bmatrix}\varepsilon_x\\ \varepsilon_y\\ \gamma_{xy}\\ \gamma_{xz}\\ \gamma_{yz}\end{bmatrix}. \tag{10}$$

Substituting Eq. (6) into Eq. (10), the expressions of internal forces and moments of the FG-GRCL panels are obtained as [2,3,9,11]

$$\begin{Bmatrix} N_x \\ N_y \\ N_{xy} \\ M_x \\ M_y \\ M_{xy} \\ T_x \\ T_y \\ T_{xy} \end{Bmatrix} = \begin{bmatrix} A_{11} & A_{12} & 0 & B_{11} & B_{12} & 0 & C_{11} & C_{12} & 0 \\ A_{12} & A_{22} & 0 & B_{12} & B_{22} & 0 & C_{12} & C_{22} & 0 \\ 0 & 0 & A_{66} & 0 & 0 & B_{66} & 0 & 0 & C_{66} \\ B_{11} & B_{12} & 0 & D_{11} & D_{12} & 0 & E_{11} & E_{12} & 0 \\ B_{12} & B_{22} & 0 & D_{12} & D_{22} & 0 & E_{12} & E_{22} & 0 \\ 0 & 0 & B_{66} & 0 & 0 & D_{66} & 0 & 0 & E_{66} \\ C_{11} & C_{12} & 0 & E_{11} & E_{12} & 0 & L_{11} & L_{12} & 0 \\ C_{12} & C_{22} & 0 & E_{12} & E_{22} & 0 & L_{12} & L_{22} & 0 \\ 0 & 0 & C_{66} & 0 & 0 & E_{66} & 0 & 0 & L_{66} \end{bmatrix} \begin{Bmatrix} \varepsilon_x^0 \\ \varepsilon_y^0 \\ \gamma_{xy}^0 \\ \phi_{x,x} \\ \phi_{y,y} \\ \phi_{x,y} + \phi_{y,x} \\ -\left(\phi_{x,x} + w_{,xx}\right)\lambda \\ -\left(\phi_{y,y} + w_{,yy}\right)\lambda \\ -\left(2w_{,xy} + \phi_{y,x} + \phi_{x,y}\right)\lambda \end{Bmatrix}, \quad (11)$$

where

$$\left(A_{ij}, B_{ij}, D_{ij}, C_{ij}, E_{ij}, L_{ij}\right) = \int_{-h/2}^{h/2} Q_{ij}\left(1, z, z^2, z^3, z^4, z^6\right) dz. \quad (12)$$

The shear force components are displayed as

$$\begin{aligned} Q_x &= H_{44} w_{,x} + H_{44}\phi_x, \\ Q_y &= H_{55} w_{,y} + H_{55}\phi_y, \\ S_x &= H_{66} w_{,x} + H_{66}\phi_x, \\ S_y &= H_{77} w_{,y} + H_{77}\phi_y. \end{aligned} \quad (13)$$

with

$$\begin{aligned} H_{44} &= -3\lambda \int_{-h/2}^{h/2} z^2 Q_{44} dz + \int_{-h/2}^{h/2} Q_{44} dz, \\ H_{55} &= -3\lambda \int_{-h/2}^{h/2} z^2 Q_{55} dz + \int_{-h/2}^{h/2} Q_{55} dz, \\ H_{66} &= -3\lambda \int_{-h/2}^{h/2} z^4 Q_{44} dz + \int_{-h/2}^{h/2} z^2 Q_{44} dz, \\ H_{77} &= -3\lambda \int_{-h/2}^{h/2} z^4 Q_{55} dz + \int_{-h/2}^{h/2} z^2 Q_{55} dz. \end{aligned} \quad (14)$$

By utilizing HSDT, the equilibrium equations of the imperfect panels under external pressure load is presented as [2,3]

$$\begin{aligned} &N_{xy,y} + N_{x,x} = 0, \; N_{y,y} + N_{xy,x} = 0, \\ &Q_{x,x} + Q_{y,y} - 3\lambda\left(S_{y,y} + S_{x,x}\right) + \left(w_{0,xx} + w_{,xx}\right)N_x \\ &+\lambda\left(T_{x,xx} + T_{y,yy} + 2T_{xy,xy}\right) + \left(w_{0,yy} + w_{,yy}\right)N_y \\ &+2\left(w_{0,xy} + w_{,xy}\right)N_{xy} + N_y/R + q = 0, \\ &M_{x,x} + M_{xy,y} - Q_x + 3\lambda S_x - \lambda\left(T_{xy,y} + T_{x,x}\right) = 0, \\ &M_{y,y} + M_{xy,x} - Q_y + 3\lambda S_y - \lambda\left(T_{y,y} + T_{xy,x}\right) = 0. \end{aligned} \quad (15)$$

The stress function is introduced, as

$$N_{xy} = -\xi_{,xy}, \; N_x = \xi_{,yy}, \; N_y = \xi_{,xx}. \quad (16)$$

The first two equations of (15) are completely satisfied, last three equations of Eq. (15) can be rewritten in the forms

$$\begin{aligned} &u_1\xi_{,xxyy} - \lambda C_{21}^*\xi_{,xxxx} - \lambda C_{12}^*\xi_{,yyyy} \\ &+u_2 w_{,xxyy} - \lambda^2 L_{11}^* w_{,xxxx} + u_3\phi_{x,xxx} \\ &+u_4\phi_{x,xyy} + u_5\phi_{y,xxy} - \lambda^2 L_{22}^* w_{,yyyy} \\ &+\left(w_{,yy} + w_{0,yy}\right)\xi_{,xx} + u_6\phi_{y,yyy} + \frac{\xi_{,xx}}{R} \\ &-2\xi_{,xy}\left(w_{,xy} + w_{0,xy}\right) + \xi_{,yy}\left(w_{,xx} + w_{0,xx}\right) \\ &+u_7\phi_{x,x} + u_8\phi_{y,y} + u_7 w_{,xx} + u_8 w_{,yy} = -q, \end{aligned} \quad (17)$$

$$\begin{aligned} &\xi_{,xxx}q_1 + \xi_{,xyy}q_2 + w_{,xxx}q_3 + w_{,xyy}q_4 \\ &+\phi_{x,xx}q_5 + \phi_{x,yy}q_6 + \phi_{y,xy}q_7 + w_{,x}q_8 \\ &+3\lambda H_{66}\phi_x - H_{44}\phi_x = 0, \end{aligned} \quad (18)$$

$$\begin{aligned} &j_1\xi_{,xxy} + j_2\xi_{,yyy} + j_3 w_{,xxy} + j_4 w_{,yyy} \\ &+j_5\phi_{x,xy} + j_6\phi_{y,xx} + j_7\phi_{y,yy} \\ &+j_8 w_{,y} + 3\lambda H_{77}\phi_y - H_{55}\phi_y = 0. \end{aligned} \quad (19)$$

The compatibility equation (9) can be also rewritten in the forms

$$\begin{aligned}&\Pi \equiv \xi_{,xxyy}k_1 + \xi_{,xxxx}A_{11}^* + \xi_{,yyyy}A_{22}^* \\ &+w_{,yy}w_{,xx} - \left(w_{,xy}\right)^2 + w_{,xxyy}k_2 + w_{,yy}w_{0,xx} \\ &-\lambda w_{,xxxx}C_{21}^* + w_{,xx}/R + w_{,xx}w_{0,yy} \\ &-2w_{,xy}w_{0,xy} - \lambda w_{,yyyy}C_{12}^* + \phi_{x,xxx}k_3 \\ &+\phi_{y,yyy}k_4 + \phi_{y,xxy}k_5 + \phi_{x,xyy}k_6 = 0.\end{aligned} \tag{20}$$

Three boundary conditions of panels are considered in this paper, as [9,11]

Boundary condition 1: Four edges of the panel are freely movable and simply supported, the rotations, deflection, moments, and forces, are (FFFF)

$$\begin{aligned}&w = 0,\ M_x = 0,\ N_{xy} = 0,\ \phi_y = 0, \\ &T_x = 0,\ N_{x0} = N_x = 0, \quad at\ \ x = 0,\ a, \\ &w = 0,\ N_{xy} = 0, M_y = 0,\ \ \phi_x = 0, \\ &T_y = 0,\ N_{y0} = N_y = 0, \quad at\ \ y = 0,\ b.\end{aligned} \tag{21}$$

Boundary condition 2: Four edges of the panel are immovable and simply supported. In this case, the rotations, deflection, moments, and forces, are (IIII)

$$\begin{aligned}&u = 0, w = 0,\ M_x = 0,\ \phi_y = 0, \\ &T_x = 0,\ N_{x0} = N_x, \quad at\ \ x = 0,\ a, \\ &v = 0,\ w = 0,\ M_y = 0,\ \phi_x = 0, \\ &N_y = N_{y0},\ \ T_y = 0, \quad at\ \ y = 0,\ b.\end{aligned} \tag{22}$$

Boundary condition 3: Four edges of the panel are simply supported. In this case, the freely movable edges $x = 0, x = a$ and immovable edges $y = 0, y = b$ (FIFI) are considered as

$$\begin{aligned}&M_x = 0, \phi_y = 0, w = 0,\ N_{xy} = 0, \\ &T_x = 0,\ N_x = N_{x0} = 0,\ \ at\ \ x = 0,\ a, \\ &v = 0, w = 0,\ \ M_y = 0, \phi_x = 0, \\ &N_y = N_{y0},\ T_y = 0, \quad at\ \ y = 0,\ b.\end{aligned} \tag{23}$$

with N_{x0}, N_{y0} are the pre-stresses in the x, y directions, respectively.

The solutions satisfied the boundary condition are chosen, as

$$\left[w, w_0\right] = \left[W, \vartheta h\right] \sin\left(\frac{m\pi}{a}x\right) \sin\left(\frac{n\pi}{b}y\right),$$

$$\begin{aligned}&\phi_x = \Phi_x \cos\left(\frac{m\pi}{a}x\right) \sin\left(\frac{n\pi}{b}y\right), \\ &\phi_y = \Phi_y \sin\left(\frac{m\pi}{a}x\right) \cos\left(\frac{n\pi}{b}y\right),\end{aligned} \tag{24}$$

where m and n are the half-wave numbers, and the imperfection size is ϑ.

The form of the stress function is referred from the stress function of cylindrical panels [8-11], as

$$\begin{aligned}\xi &= \sin\left(\frac{m\pi}{a}x\right) \sin\left(\frac{n\pi}{b}y\right) \xi_{s,p,c}^1 \\ &+ \cos\left(2\frac{m\pi}{a}x\right) \xi_{s,p,c}^2 + \cos\left(2\frac{n\pi}{b}y\right) \xi_{s,p,c}^3 \\ &+ y^2 N_{x0}/2 + x^2 N_{y0}/2,\end{aligned} \tag{25}$$

where the subscripts s, p and c denote the sinusoidal, parabola, and cylindrical panels.

Substituting Eq. (24) into the Eq. (20), then, the like Galerkin method is applied, as

$$\begin{aligned}&\int_0^b \int_0^a \Pi \sin\left(\frac{m\pi}{a}x\right) \sin\left(\frac{n\pi}{b}y\right) dxdy = 0, \\ &\int_0^b \int_0^a \Pi \cos\left(2\frac{m\pi}{a}x\right) dxdy = 0, \\ &\int_0^b \int_0^a \Pi \cos\left(2\frac{n\pi}{b}y\right) dxdy = 0,\end{aligned} \tag{26}$$

leads to the forms

$$\begin{aligned}\xi^1 &= \frac{\left(\frac{m\pi}{a}x\right)^2 \left(W + 2\vartheta h\right) W}{32 A_{22}^* \left(\frac{n\pi}{b}y\right)^2} + f^2 W, \\ \xi^2 &= f^3 \Phi_x + f^4 \Phi_y + f^5 W, \\ \xi^3 &= \frac{\left(\frac{n\pi}{b}y\right)^2 \left(W + 2\vartheta h\right) W}{32 A_{11}^* \left(\frac{m\pi}{a}x\right)^2} + f^1 W.\end{aligned} \tag{27}$$

Substituting the solution forms and the stress function forms into the equilibrium equations (17)-(19), and the Galerkin method is applied, leads to

$$
\begin{aligned}
&(W+h\vartheta)N_{x0}\kappa^1+(W+h\vartheta)N_{y0}\kappa^2+\Phi_x\kappa^3+\Phi_y\kappa^4+W^3\kappa^7\\
&+\Phi_x(W+h\vartheta)\kappa^5+\Phi_y(W+h\vartheta)\kappa^6+W(W+h\vartheta)(W+2h\vartheta)\kappa^8\\
&+(W+2h\vartheta)W\kappa^9+W(W+h\vartheta)\kappa^{10}+N_{y0}\kappa^{11}+W\kappa^{12}+q\kappa^{13}=0,\\
&\Phi_x\lambda^1+\Phi_y\lambda^2+W(W+2h\vartheta)\lambda^3+W\lambda^4=0,\\
&\Phi_x\lambda^5+\Phi_y\lambda^6+W(W+2h\vartheta)\lambda^7+W\lambda^8=0.
\end{aligned}
\tag{28}
$$

Solve the two end equations of Eq. (28), Φ_x,Φ_y are obtained as

$$
\begin{aligned}
\Phi_x&=(W+2h\vartheta)We^1+We^2,\\
\Phi_y&=(W+2h\vartheta)We^3+We^4.
\end{aligned}
\tag{29}
$$

The load-deflection relation is determined by substituting Φ_x,Φ_y into the first of (28), as

$$
\begin{aligned}
&\bar{W}^3h^2\kappa^7+\upsilon_1N_{x0}(\bar{W}+\vartheta)\kappa^1\\
&+(\bar{W}+2\vartheta)\bar{W}(\bar{W}+\vartheta)h^2e^6\\
&+\bar{W}e^8+\bar{W}(\bar{W}+\vartheta)he^5\\
&+(\bar{W}+2\vartheta)\bar{W}e^7+\frac{\upsilon_2N_{y0}\kappa^{11}}{h}\\
&+\upsilon_2N_{y0}(\bar{W}+\vartheta)\kappa^2+q\frac{\kappa^{13}}{h}=0,
\end{aligned}
\tag{30}
$$

where the FFFF boundary condition is obtained by applying $\upsilon_1=0$ and $\upsilon_2=0$. The IIII boundary condition is obtained by applying $\upsilon_1=1$ and $\upsilon_2=1$. The FIFI boundary condition is obtained by applying $\upsilon_1=0$ and $\upsilon_2=1$.

For immovable edges, $v=0$ at the edges $y=0,b$ and $u=0$ at the edges $x=0,a$ the immovable condition at all edges is satisfied with the average conditions as

$$
\int_0^a\int_0^b v_{,y}dydx=0,\quad \int_0^b\int_0^a u_{,x}dxdy=0.
\tag{31}
$$

The expressions of N_{x0},N_{y0} can be determined from Eq. (31), as

$$
\begin{aligned}
N_{x0}&=\varsigma^1\Phi_x+\varsigma^2\Phi_y\\
&+\varsigma^3W(W+2h\vartheta)+\varsigma^4W,
\end{aligned}
\tag{32}
$$

$$
\begin{aligned}
N_{y0}&=\varsigma^5\Phi_x+\varsigma^6\Phi_y\\
&+\varsigma^7W(W+2h\vartheta)+\varsigma^8W.
\end{aligned}
\tag{33}
$$

Substituting Eqs. (32) and (33) into Eq. (30) the relation between q and $\bar{W}=W/h$ is written by

$$
\begin{aligned}
q=&-\frac{h}{\kappa_{s,p,c}^{13}}\times\\
&\times\begin{pmatrix}
\bar{W}^3h^2\kappa^7+\gamma^2\bar{W}(\vartheta+\bar{W})\\
+\gamma^1(2\vartheta+\bar{W})\bar{W}(\vartheta+\bar{W})\\
+\bar{W}e^8+\gamma^4\bar{W}+(2\vartheta+\bar{W})\bar{W}e^7\\
+\gamma^3(2\vartheta+\bar{W})\bar{W}
\end{pmatrix}.
\end{aligned}
\tag{34}
$$

3. Results and discussions

To check or prove the accuracy of the present analysis, the postbuckling curves of externally pressured FG-GRCL plates are compared with the previous results of Shen et al. [1] in Fig. 2. Perceived that the good agreement is presented, two results coincide together.

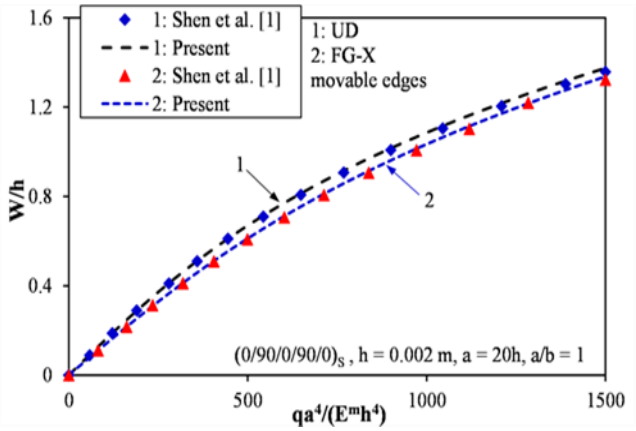

Fig. 2. Comparison of the postbuckling curves of FG-GRCL plates with previous results

The postbuckling curves of three-panel types are compared in Figs. 3a,b,c with three types of

boundary condition. While the postbuckling bearing capacities are very close together in the case of the FFFF boundary condition (Fig. 3a), the postbuckling curves of the parabola panel show superiority over the other two panel types with FIFI and IIII boundary conditions (Figs 3b,c). Figs. 3d,e compare the postbuckling bearing capacities of FG-X $(0)_{10}$ parabola and sinusoidal panels with three cases FFFF, FIFI, and IIII. As can be seen, the snap-through can be recognized only for perfect FIFI panels for both parabola and sinusoidal panels. The postbuckling curves of IIII panels are significantly higher than FIFI and FFFF panels in the large deflection domain. The postbuckling curves of FIFI and IIII panels coincide In the small deflection domain.

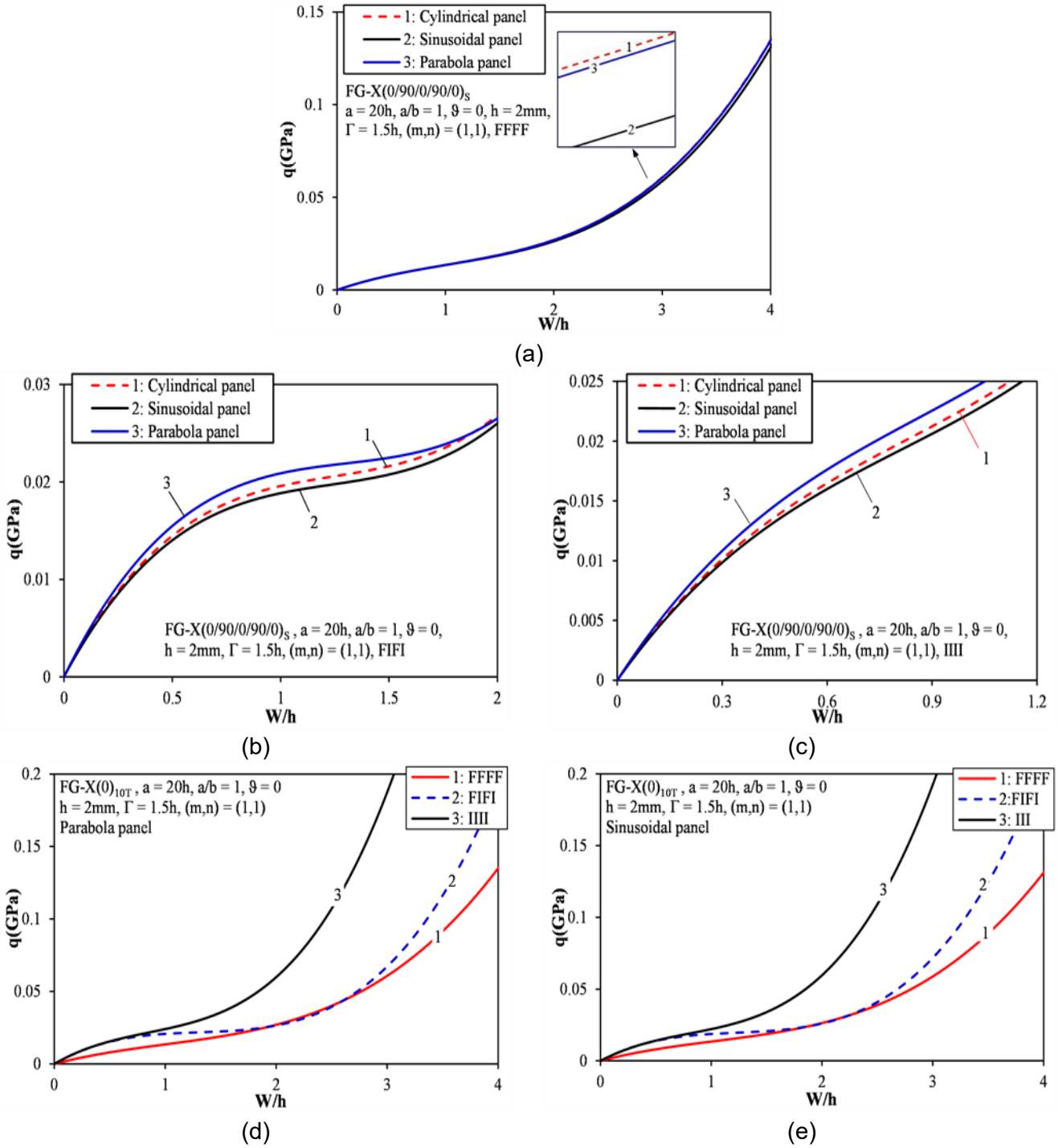

Fig. 3. Effects of panel type and boundary condition on the postbuckling curves of panels

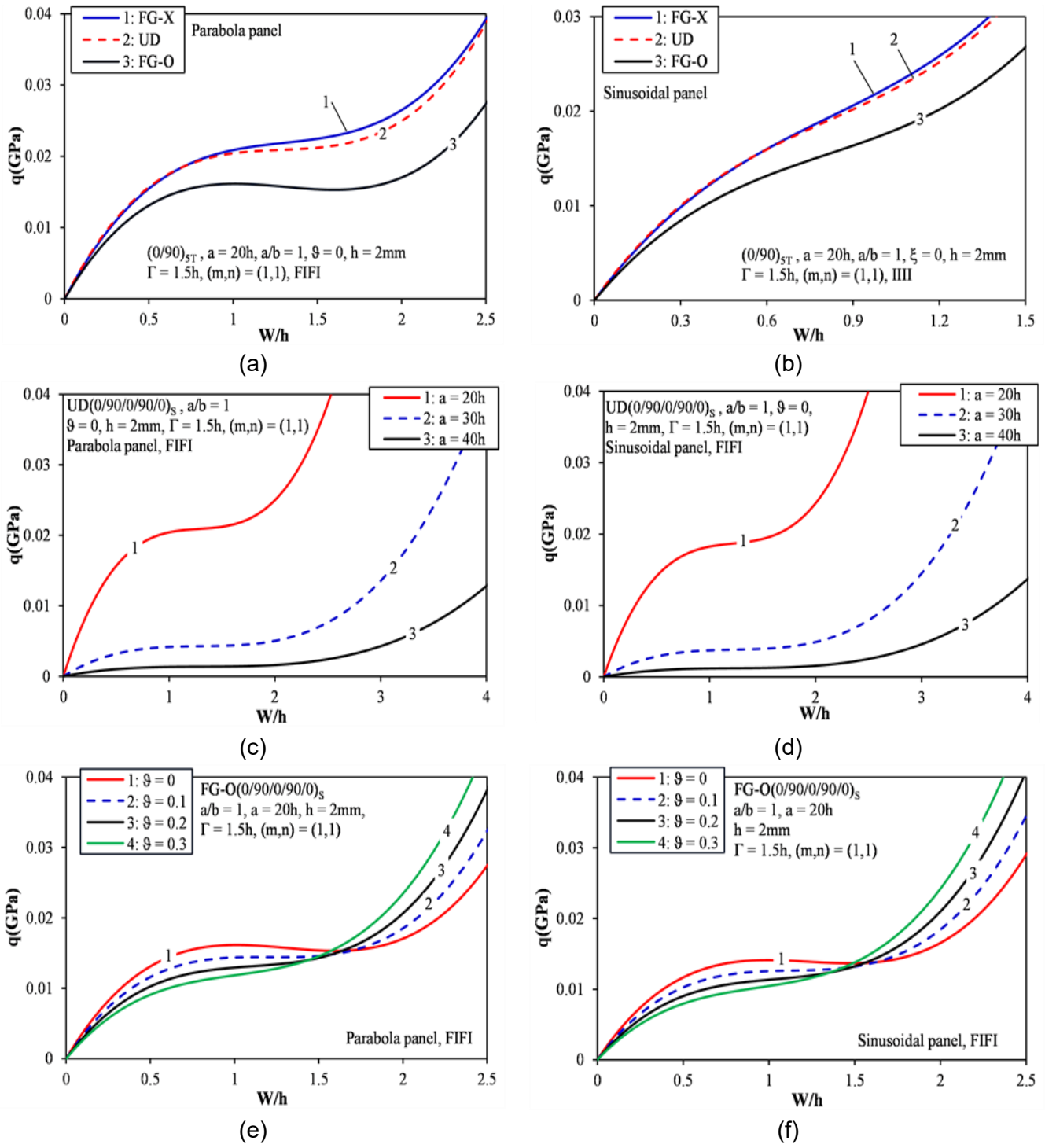

Fig. 4. Effects of graphene distribution types, geometrical parameters and imperfection sizes on the postbuckling curves of panels

Figures 4a, and b evaluate the influences of the distributions (UD, FG-O, and FG-X) on the postbuckling behavior of the $(0/90)_{5T}$ FG-GRCL parabola and sinusoidal panels. The postbuckling bearing capacity of the FG-O type is the smallest and that of the FG-X type is the largest.

In the case of parabola panels, the snap-through can be clearly observed for the FG-O panels. The influences of the a/h on the postbuckling curves of FIFI UD $(0/90/0/90/0)_S$ parabola and sinusoidal panels are displayed in Figs. 4c, d. The postbuckling load-carrying capacity for thinner panel is strongly reduced in both panel types, and this difference becomes

larger as the deflection increases. Figures 4e and f display the influences of imperfection on the postbuckling curves of FG-O $(0/90/0/90/0)_S$ FIFI parabola and sinusoidal panels. When the imperfect deflection rises, the snap-through lowers slightly and then vanishes. The postbuckling bearing capacities of imperfect cases are larger than those of perfect cases if the sufficiently large deflection is applied.

4. Conclusions

The external pressured postbuckling of the parabola, sinusoidal, and cylindrical GRCL panels is calculated and discussed. To overcome the mathematical difficulty of the complex curvature, the approximate technique is utilized to obtain the stress function of panels. The investigations give meaningful remarks:

1) The postbuckling bearing capacities are very close together in the case of the FFFF boundary condition, the postbuckling bearing capacities of the parabola panel show superiority over the other two panel types with FIFI and IIII boundary conditions.

2) The snap-through can be recognized only for perfect FIFI panels for both parabola and sinusoidal panels.

3) When the imperfect deflection rises, the snap-through lowers slightly and then vanishes.

References

[1] H.S. Shen, Y. Xiang, F. Lin. (2017). Nonlinear bending of functionally graded graphene-reinforced composite laminated plates resting on elastic foundations in thermal environments. *Composite Structures*, 170, 80-90.

[2] H.S. Shen, Y. Xiang, Y. Fan. (2018). Postbuckling of functionally graded graphene-reinforced composite laminated cylindrical panels under axial compression in thermal environments. *International Journal of Mechanical Sciences*, 135, 398-409.

[3] H.S. Shen, Y. Xiang, J.N. Reddy. (2019). Thermal postbuckling behavior of FG-GRC laminated cylindrical panels with temperature-dependent properties. *Composite Structures*, 211, 433-442.

[4] Y. Fan, Y. Xiang, H.S. Shen. (2019). Nonlinear forced vibration of FG-GRC laminated plates resting on visco-Pasternak foundations. *Composite Structures*, 209, 443-452.

[5] M. Mirzaei, Y. Kiani. (2017). Isogeometric thermal buckling analysis of temperature dependent FG graphene reinforced laminated plates using NURBS formulation. *Composite Structures*, 180, 606-616.

[6] Y. Kiani. (2018). NURBS-based isogeometric thermal postbuckling analysis of temperature dependent graphene reinforced composite laminated plates. *Thin-Walled Structures*, 125, 211-219.

[7] Y. Kiani. (2018). Isogeometric large amplitude free vibration of graphene reinforced laminated plates in thermal environment using NURBS formulation. *Computer Methods in Applied Mechanics and Engineering*, 332, 86-101.

[8] V.H. Nam, D.T. Dong, C.V. Doan, N.T. Phuong. (2022). Nonlinear Thermo-Electro-Mechanical Buckling of Higher-Order Shear Deformable Stiffened FG-GRC Laminated Plates. *International Journal of Applied Mechanics*, 14(06), 2250051.

[9] V.H. Nam, D.T. Dong, C.V. Doan, N.T. Phuong. (2022). Nonlinear buckling of axially compressed FG-GRCL stiffened cylindrical panels with a piezoelectric layer by using Reddy's higher-order shear deformation theory. *Polymer Composites*, 43(11), 7952-7966.

[10] N.T. Phuong, D.T. Dong, C.V. Doan, V.H. Nam. (2022). Nonlinear buckling of higher-order shear deformable stiffened FG-GRC laminated plates with nonlinear elastic foundation subjected to combined loads. *Aerospace Science and Technology*, 127, 107736.

[11] N.T. Phuong, D.T. Dong, V.C. Doan, V.H. Nam. (2023). Nonlinear buckling of stiffened

FG-GRCL cylindrical panels under axial compression with the uniformly distributed temperature variation. *The European Physical Journal Plus*, 138, 234.